IJES *Iranian Journal of Earth Sciences*
Vol. 13, No. 2, 2021, 148-158.

Ground-motion simulation for the 2017 Mw7.3 Ezgeleh earthquake in Iran by using the Empirical Green's Function Method

Maryam Pourabdollahi[1], Arezoo Dorostian[1], Habib Rahimi*[2], Attieh Eshaghi[3]

1. Department of Geology, North Tehran Branch, Islamic Azad University, Tehran, Iran
2. Institute of Geophysics, University of Tehran, Tehran, Iran
3. Road, Housing and Urban Development Research Center, BHRC, Tehran, Iran

Received 16 November 2019; accepted 22 May 2020

Abstract

The aim of this study is to investigate the strong ground motion generation of destructive earthquake in Kermanshah with the moment magnitude of 7.3 using Empirical Green’s function (EGF) method. To simulate the ground-motion can be helpful for understanding seismic hazard and reduce fatalities due to lack of real ground motion. We collected the seismograms recorded at seven strong motion stations with good quality to estimate the source parameters at frequencies between 0.1 and 10.0 Hz. By minimizing the root-mean-square (rms) errors to obtain the best source parameters for the earthquake. The earthquake fault was divided into seven sub-faults along the strike and seven sub-faults along the slope. The asperity of 21×10.5 km was obtained. The rupture starting point has been located in the northern part of the strong motion seismic area. The coordinates of the rupture starting point indicate that the rupture propagation on the fault plan was unilateral from north to south. The simulated ground motions have a good correlation with observed records in both frequency and time domain. The results are in well agreement with the Iranian code of practice for seismic resistant design of buildings, however, the calculated design spectrum of Sarpol-e Zahab station is higher than the design spectrum of the Iranian code which suggest that the Iranian code may need to be re-evaluated for this area.

Keywords: *Empirical Green’s Function Method, 2017 M7.3 Ezgeleh Earthquake, Simulation, Strong Motion*

1. Introduction

The Zagros convergent boundary, a young continental collision zone, has produced a huge mountain range during collision of Arabian plate and Central Iran plate which is a part of Eurasian plate (Dewey et al. 1973). The structure trend of Zagros is approximately NW–SE and its Shortening absorbs about one-third of the Arabia–Eurasia convergence (Jackson et al. 1995). The Mountain Front Fault (MFF), which is located in the southwest of the Zagros (Fig 1), is an overthrust fault and produce the most seismic moment release (Vajedian et al. 2018; Poorbehzadi et al. 2019; Yazdi et al. 2019). Studies of the magnitude and distribution of earthquakes such as the Mw 7.3 and the Mw 6.2, 2006 Silakhur earthquake show high seismicity with medium and large earthquake magnitudes within the Zagros. Ezgeleh earthquake was the largest instrumental earthquake which occurred on November 12, 2017 at 21:48:16 local time. Examination of the earthquake fault mechanism shows that the earthquake had a dip-slip mechanism due to the thrust faulting with a dip-slip component at low crust depth (Fig 1). The main shock and its aftershocks elongated in a north–south direction distributed in an area of 120 km × 150 km, west of the main shock (Yazdi et al. 2017; Vajedian et al. 2018). This devastating earthquake occurred in the Zagros zone, causing many deaths and financial losses, with death toll of 620, more than 7000 injured, and about 70000 homeless (Bazoobandi et al. 2016; Ahmadi and Bazargan - Hejazi 2018; Miyamjima et al. 2018). The earthquake had two foreshocks with a magnitude greater than 4.5 and it also had more than 100 aftershocks with a magnitude less than 5.4 in the first month after the main shock. The area has also witnessed devastating earthquakes in recent years. Historically recorded earthquakes included the April 958 earthquake of M6.4, the April 23 1008 earthquake of M7 (56000 deaths), and June 1872 (1500 deaths) (Ambraseys and Melville 1982).

In recent years, studies have been conducted in Iran to simulate strong motion records. Nicknam et al. (2009) simulated the records of strong motion related to the Silakhor earthquake using the EGF method and Genetic Algorithm. The genetic algorithm has been used in their study to reduce the difference between simulated records and actual records. Riahi et al. (2015) studied the Bam earthquake scenario using EGF and they used very small earthquakes to simulate the main earthquake. Despite the large magnitude of the earthquake in Kermanshah, no serious study has yet been conducted to simulate this earthquake. In the study area, Miyamjima et al. (2018) investigated the site effect for nearby stations that recorded the Ezgeleh main shock. They reported that the maximum Peak Ground Acceleration (PGA) at Sarpol-e Zahab station 39 km away was about 681, 582 and 404 cm/s^2 for the vertical and horizontal components, respectively. Using the Interferometric Synthetic Aperture Radar (InSAR) data, Feng et al. (2018) estimated the centroid depth for the Ezgeleh earthquake at 14.5 km.

---

*Corresponding author.
E-mail address (es): rahimih@ut.ac.ir

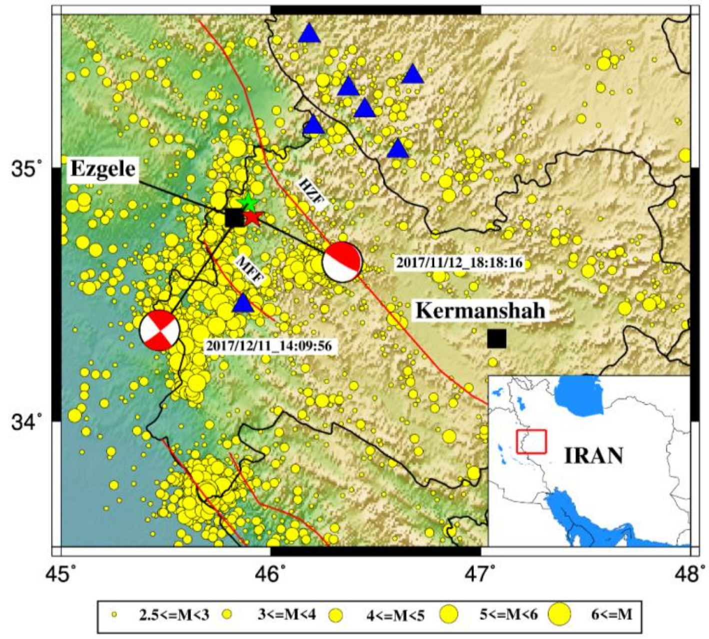

Fig 1. Spatial distribution of the seismic events in the study area. The red stars represent the main earthquake and the green star represents the selected aftershock. The blue triangles show the selected stations used in this study. The black rectangles represent the center of Kermanshah and Ezgele cities. The yellow circles represent the region's seismicity from 2006 to 2019. The red lines are the HZF (High Zagros Fault) and MFF (mountain front faulting) fault.

The source length and width of this earthquake was reported 16 and 4 km, respectively (Feng et al. 2018).

Due to the increase of destructive earthquakes in Zagros area, seismic hazard assessment and design of earthquake resistant structures in order to reduce the damages is inevitable. Estimation of these two parameters (seismic hazard assessment and design of resistant structures) require strong ground motion records. Regardless of the increasing number of seismometers throughout Iran, there is a lack of good strong-motion records within this zone. So, strong ground-motion simulation using EGF method can provide valuable information for seismic hazard assessment.

Today, the numerous methods are used for strong motion simulation such as stochastic simulation of high-frequency ground motion; Composite source modeling technique; Empirical Green’s Function (EGF) method and so on. Among these methods, the EGF method was chosen for the present study, because this method uses a small earthquake (aftershock or foreshock) to simulate the main earthquake. In this method, due to the similarity between the path and site effects of small events and the main event, it is not necessary to calculate the path and site effects. The EGF method was first introduced by Hartzell (1978) and later formulated by (Irikura 1986). This method has been established on the basis that the strong motion in a building is derived from the principle of the sum of a series of motions, which are the result of single fractures of small fragments on a fault plane with certain time delay. This method uses smaller earthquakes to calculate the site effect and how the wave propagates (Hartzell 1978; Irikura 1986).

In this study, it is attempted to estimate the Ezgeleh earthquake scenario by EGF method using small events (aftershocks). In order to simulate the Ezgeleh earthquake, seven accelerograms were processed. Compared to other studies, this study examines the impact of all the parameters involved in modeling and finally, the best parameters are selected based on the least misfit error; then, based on these selected parameters the simulation and modeling are performed. Selection parameter based on the least misfit error is considered due to the variation of source parameters obtained in different studies. A review of the studies on the source mechanism of Ezgeleh earthquake shows that, the estimated parameters of source are not unique in different studies. For example, variation of shear wave velocity and consequently rupture velocity is seen in different studies. For instance, Ding et al. (2018) have estimated the average speed of 2.5 km/s for rupture velocity, while Gombert et al. (2019) reported the estimated value of ~ 3 km/s.

2. Data and analysis

To simulate strong ground motion of Ezgeleh earthquake, the data recorded at seven stations from Iran Strong Motion Network (ISMN) of Housing and Urban

Development Research Center (BHRC) which were distanced between 39 and 92 were processed. The main shock with magnitude Mw=7.3 was located at 34.88 N° and 45.84 E° and depth 18 km. The focal mechanism of this earthquake has been shown in Figure 1. In order to select the aftershock for simulation of the main shock, we checked all the aftershocks recorded by ISMN from 12, Nov 2017 to 31, Dec 2017. Most of the checked aftershocks were recorded just at two or three stations. We selected one aftershock that has the highest number of recordings. This selected aftershock is an earthquake with the magnitude of 4.6, dip-slip mechanism and focal depth of 20 km that was located at 35.08 N° and 45.84 E°. Focal mechanism of this aftershock is different from the main shock (Fig 1), however, due to the lack of good recorded waveforms at other stations, we had to use this event as an input aftershock. Table 1 shows the specifications of the selected stations.

Table 1. Parameters of the strong motion stations used in this study.

Station	Long (deg)	Lat (deg)	Elevation (m)	Hypocentral distance(km)
Degaga	46.44	35.22	1295	67
Marivan	46.18	35.51	1340	82
Nosood	46.20	35.61	1288	47
Palangan	46.60	35.06	1250	69
Sarv Abad	46.39	35.31	1025	70
Sarpolezahab	45.86	34.45	558	39
Shoeisheh	46.67	35.35	1457	92

To perform EGF simulation, first the selected strong motion data should be corrected. For this purpose, the baseline correction is used to remove the short and long period errors from accelerograms. Correction of these errors have been done by subtracting a best-fit parabola from the accelerogram before integrating velocity and displacement or by applying high-pass filters on data (Cramer 1996). Alternatively, for digital accelerograms with pre-event, it is possible to remove from the entire signal the average value calculated only on the pre-event portion. Records used in this study are corrected using standard processing techniques (Boore 2003). Additionally, visual inspection is used to analyze each component of the strong motion records.

During the baseline correction, we applied a highpass filter with corner frequency of 0.05 to remove the long period noise effect. To improve the results, accelerograms with high signal-to-noise ratio were selected and processed (Fig 2). Signal to noise ratio is defined as follows (Theodulidis and Brad 1995):

$$SNR=(S(f)/\sqrt{t1})/(N(f)/\sqrt{t2}) \qquad (1)$$

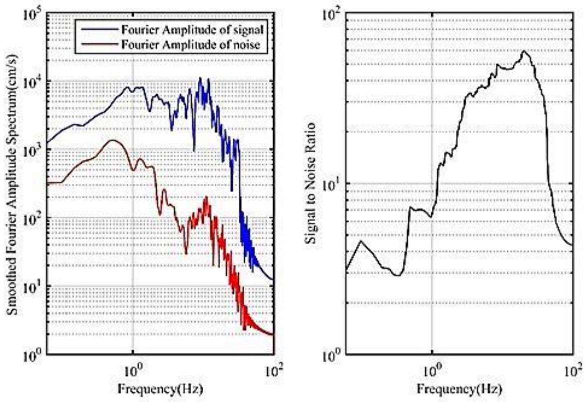

Fig 2. The signal to noise ratio of Degaga record (main shock). Left figure shows the Fourier amplitude of signal and noise for Degaga record and right figure shows signal to noise ration.

3. EGF Method

Hartzell (1978) introduced the method of investigating major earthquakes using the foreshock or aftershock (small events) entitled as the Empirical Green's Function (EGF). Niño et al. (2018) improved this method by using a source which defined by two corner frequency and two-stage summation scheme. The basic idea of EGF is that the source, path, and site information that is present in the main event are also present in the small event. Green's empirical function approach has the advantage of taking into account the complex path, site effects, and complexity of the inhomogeneous structure of the Earth between the source and the recording site. In the EGF simulation, the fault plane is considered as a rectangular plane divided into N×N components (Irikura 1986) (Fig 3). The relationship between main event and small event parameters has been defined by the scaling relationships of Kanamori and Anderson (1975). In this method, information about the slip velocity of source time function of the small event is not necessary. To model the target earthquake rupture using the EGF method, the major fault rupture must be uniformly subdivided into sub-faults causing the small earthquakes.

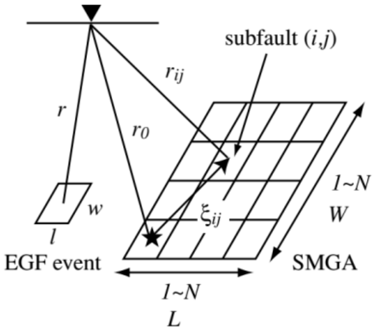

Fig 3. Fault surface of large and small events, defined as L×W and l×w respectively (Irkuria et al. 1997).

Therefore, there is a need for similarity relationships between the source parameters of the target event and the small event. Two similarity relationships have been proposed by (Irikura 1986). The first similarity relationship is for the parameters such as fault area, magnitude and the other is the scaling relationship for the source spectrum. The scaling relationship of the source parameter derived from the studies of (Kanamori and Anderson 1975) is as follows:

$$\frac{L}{l}=\frac{W}{w}=\frac{T_r}{t_r}=\frac{D}{d}=N \tag{2}$$

Here, for major earthquake, L and W are the length and width of the fault. Tr is rise time and D is the average slip of mainshock. Lowercase letters are for aftershock.

$$\frac{A_0}{a_0}=(\frac{M_0}{m_0})^{1/3}=N \tag{3}$$

Where, A_0 and a_0 are the flat part at the high frequency portion of the acceleration spectrum of the large (major) and small (aftershock) earthquakes respectively. Boore (1983) provided a relationship for the corner frequency (fc) in which fc is directly proportional to the third root of the stress drop and inversely proportional to the third root of the seismic moment (M_0). If the stress drop is considered to be constant for the main event and the aftershock, then the scaling relation between corner frequency and seismic moment is presented by following equation:

$$\frac{f_{cm}}{f_{ca}}=(\frac{m_0}{M_0})^{1/3}=N^{-1} \tag{4}$$

Where, f_{cm} and f_{ca} are respectively the corner frequencies of the major and aftershock events. However, the condition that the stress drop is constant over a wide range of sizes is not always true. Irikura (1986) introduced the general relationship for a model with a W2 source spectrum where the stress drop is not equal, as follows:

$$\frac{L}{l}=\frac{W}{w}=\frac{T_r}{t_r}=(\frac{M_0}{Cm_0})^{1/3}=N \tag{5}$$

$$\frac{D}{d}=\frac{A_0}{a_0}=CN \tag{6}$$

Where, C is equal to the difference between the stress drops of the two earthquakes (Fig 3). The target earthquake record, U(t), is obtained from the sum of the Green's functions of each component of the fault (u(t)) in relationships 6 and 7.

$$U(t)=\sum_{i}^{N_x}\sum_{j}^{N_w}\frac{r}{r_{ij}}C.(F(t)*u(t-t_{ij})) \tag{7}$$

$$t_{ij}=\frac{r_{ij}-r_0}{V_s}+\frac{\xi_{ij}}{V_r} \tag{8}$$

Where, N_x and N_w are the number of sub-faults along the strike and dip. r and r_{ij} are the distance of the recording station from the aftershock and the element (i, j) respectively. F(t) is the filler function that corrects the time difference function of the rupture velocity between the small and large events. In equation 8, V_s and V_R are the shear wave velocity around the source and the rupture velocity, respectively and r_0 is the focal distance of the main earthquake. ξ_{ij} represents the distance between element (i, j) and the starting point of the fault.

In order to perform the simulation process, it is necessary to determine the input parameters including fault parameters, asperity ratio, fracture starting point, stress drop, rise time, shear wave velocity and rupture velocity. For this purpose, the above-mentioned parameters have been studied and for each of the parameters and their possible values, the difference of simulated and observed response spectra have been calculated and then the most desirable values have been selected. To determine these unknown parameters, Equation 9 was used to calculate the difference between simulated and observed response spectra. For this purpose, to determine each parameter, all other parameters are assumed to be constant. Then the variable parameter, defined in a possible range, changes with a certain step and the spectrum of simulated record is fitted to the actual record for all stations. Using equation 9, the error value is determined for each record. Finally, by averaging the errors obtained for all stations, the lowest error value is selected and the parameter value is determined.

$$RMSE=\left[\frac{1}{N}\sum_{i=1}^{N}\left\{\frac{(a_f(i)-a_s(i))}{a_f(i)}\right\}^2\right]^{1/2} \tag{9}$$

where, $a_f(i)$ and $a_s(i)$ are the i-th values of the actual response spectrum and simulation with the sample N. Determination of the input parameters are explained in the following section.

4. Results

In order to ground-motion simulation, at the first step, it is necessary to extract accurate source parameters from other studies. Since the authors have given different results for source parameters, we used the RMS method (Equation 9) to find the best parameters with lowest error. In the following we describe the parameters in more detail.

4.1. Asperity ratio and number of sub faults

The fault asperity here refers to the main fault asperity, defined by Somerville et al. (1999) as a fault area that exceeds the mean slip of the main event. Miyake et al. (2003) showed that this parameter plays a key role in the simulation process. Usually, strong ground motions are associated with slip heterogeneity rather than the entire rupture region and the whole seismic moment (Irikura and Miyake 2011). For this reason, the asperity is used to investigate the characteristics of the source model. In previous studies on Ezgeleh earthquake (Ding et al. 2018; Feng et al. 2018), the amount and mode of slip on the causative fault have been determined and the rupture length of 48 km and width of 32 km have been reported. The highest reported asperity is 16 km long and 6 km wide. In our study, a range from 0.4 to 10 was considered to determine the dimensions of each sub-fault and finally, using Equation 9, the dimensions of each sub-fault were explored 1.5 km along with the dip (D_w) and 3 km for Strike (Table 2). Also, to estimate the asperity, the area that generated the strong motion was divided into seven blocks along the strike (N_x) and seven blocks along with the dip (N_w). For each strong motion block time series were simulated and the best result (with smallest error) was obtained (Table 2). Finally, the asperity dimensions were determined as 21 × 10.5 km.

Table 2. Estimated input source parameters used for the grid search.

	Dx	Dw	Nx	Nw	C	Rise time	Vs	Vr
Search range	0.5 to 10	0.5 to 10	5 to 15	5to 15	0.5 to 3.5	0.01 to 2.5	2.8 to 4.2	2 to 3.4
Step	0.5	0.5	1	1	0.1	0.01	0.1	0.1
Estimated value	3	1.5	7	7	2	0.4	3.6	2.4

4.2. Determination of rupture starting point

Here, the fracture start point that indicates the direction of fracture propagation is determined by a grid search method. To determine the fracture starting point, each sub-fault has been considered as the beginning of fault rupture and the rupture starting point has been estimated according to the root mean square (rms) of the theoretical and observed response spectra. The search of the fracture start point was performed on a 7 × 7 grid, where point 4 and point 6 had the smallest error along with the dip and strike, respectively.

4.3. Determination of stress drop

The C value is considered as the stress drop between the large and a small event. The following equation is used to determine this parameter.

$$C = \left(\frac{M_0}{m_0}\right)\left(\frac{f_{cm}}{f_{ca}}\right)^3 \qquad (10)$$

Where, M_0 and f_{cm} are seismic moment and corner frequency of the large event respectively, and m_0 and f_{ca} are seismic moment and corner frequency of the small event as well. According to Equation 10, the value of stress drop ratio is 1.78. In order to improve the stress drop estimation, the amount of stress drop between 0.5 and 3.5 with step of 0.1 was investigated according to relationship (10) (Table 2) and eventually value 2 was chosen for simulation.

4.4. Determination of rise time

Rise time is defined as the length of the filter function (F in Equation 7). This parameter shows the temporal function of the slip velocity on the surface (Miyake et al. 2003). To determine the rise time, the relationship introduced by Somerville et al. (1999) was used. The rise time of 0.4 seconds was considered in this study (Table 2).

4.5. Determination of the S-wave velocity in the region

Shear wave velocity is an effective parameter in simulating of the strong motion by EGF method. We first used previous studies done in the west of Iran to estimate the shear wave velocity in the region. Initially, shear wave velocity was assumed to be 3.5 km/s (Tatar 2001; Kaviani 2004). In order to improve the shear wave velocity estimation and to select the optimal solution, shear wave velocity was considered in the range of 2.5 to 4 km/s. Finally, by using Equation 9, this value was estimated at 3.6 km/s (Table 2).

4.6. Determination of rupture velocity

Fault rupture velocities vary in different studies. For example, Bouchon et al. (2006) considered this value to be 0.92 of the S-wave velocity, and Madariaga (1976) considered it as the 0.75 of the S-wave velocity. In this study, the rupture velocity varied between two values of 2 to 3.5 km/s and eventually the velocity of 2.4 km/s was chosen (Table 2).

4.7. Determination of the mechanism of the main event and aftershock

Tables (3) and (4) were used to determine the focal mechanism of the earthquake, which is one of the most important input parameters for simulation by the EGF method, and then the optimal values were determined using the Equation 9 (Figs 4 and 5). After finding the best input source parameters, we simulated 7 ground motions from 7 real waveforms. Figures 6 to 12 show the comparison between the observed and simulated three components accelerograms and their response spectra for the selected stations.

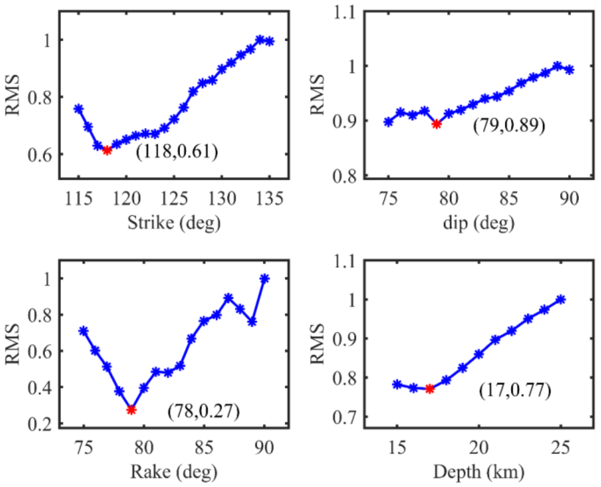

Fig 4. Determination of strike, dip, rake and depth parameters for the main earthquake. Blue stars are selected values for each parameters and red stars are the best value (minimum RMS).

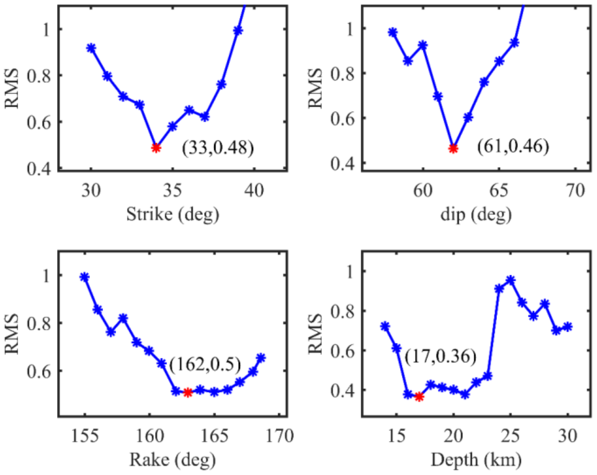

Fig 5. Determination of strike, dip, rake and depth parameters for aftershocks. Blue stars are selected values for each parameters and red stars are the best value (minimum RMS).

Table 3. Main shock's parameters reported by different agencies.

Reference	Strike	Dip	Rake	Depth (km)	M_0
USGS	129	79	78	21.5	1.124e+20
NEIC	122	79	78	21.5	1.12 e+20
IRSC	121	83	82	17.9	1.59 e+20
Search range	115-135	75-90	75-90	15-25	
Estimated value	118	79	78	17	

Table 4. Aftershock's parameters reported by different agencies.

Reference	Strike	Dip	Rake	Depth (km)	M_0
USGS	36	62	164	21.5	1.58e+17
NEIC	36	61	164	19.5	1.59e+17
IRSC	34	65	159	23.4	2.17e+17
Search range	30-40	58-70	155-170	14-25	
Estimated value	33	61	162	17	

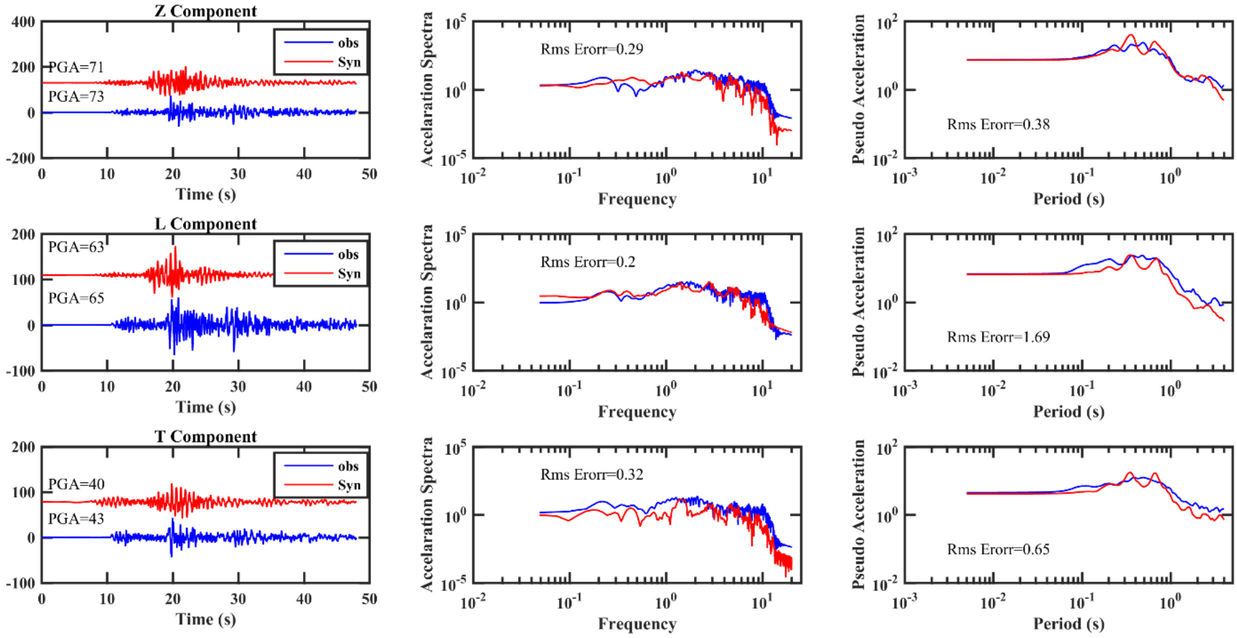

Fig 6. Observed (obs) and simulated (Syn) time series for three components of Degaga station (left column); Acceleration spectrum (middle column) and response spectrum (right column) also shown for observed (blue lines) and simulated (red lines) time series.

5. Discussion and Conclusion

In the present study, the Ezgeleh earthquake source parameters were estimated using ground strong motion simulation by EGF method in the frequency range of 0.1 to 10 Hz. For this purpose, the initial parameters for simulation were obtained on the basis of grid search approach.

The results show that the asperity length is 21 km and its width is 10.5 km. Examination of the rupture start point revealed that the rupture start point coordinates are on the north side of the rupture plane and the fracture has a north-south trend. The depth of the rupture starting point was estimated to be 15.5 km. Feng et al. (2018) investigated the transient surface deformation created by the Ezgeleh earthquake using InSAR measurements. They introduced an asperity model for this earthquake, which is in good agreement with our study. The best mechanism obtained from other studies (based on the RMS method) shows that the fault has the direction, dip and rake of 118, 79 and 78 degrees, respectively.

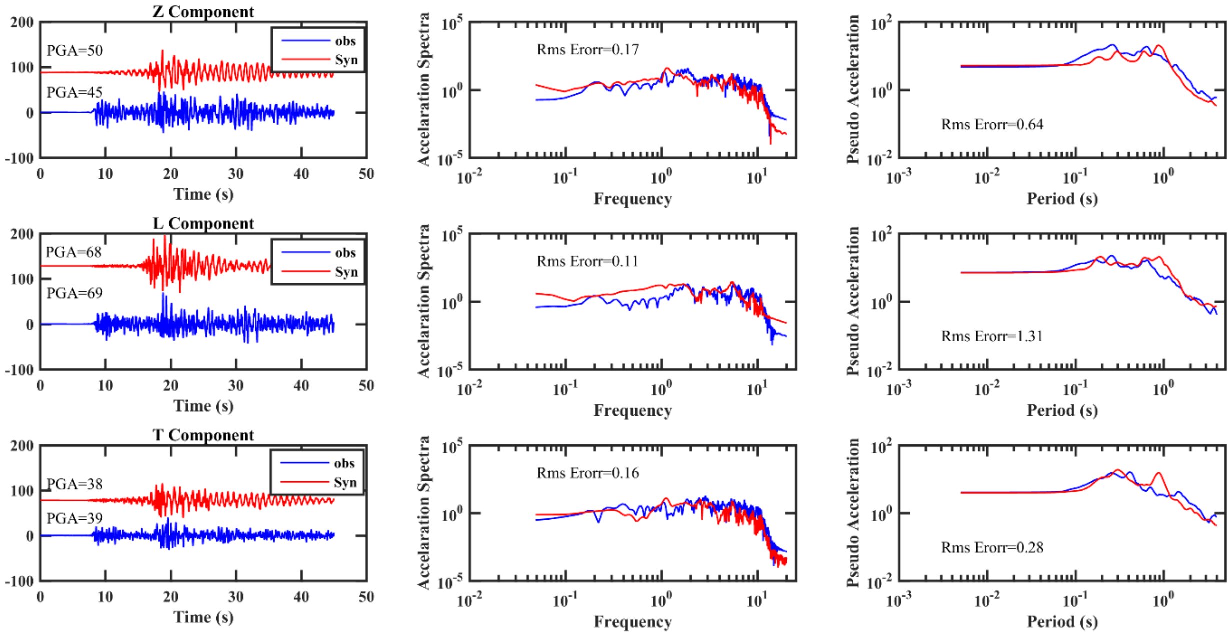

Fig 7. Observed (obs) and simulated (Syn) time series for Marivan station (left column); Acceleration spectrum (middle column) and response spectrum (right column) also shown for observed and simulated time series.

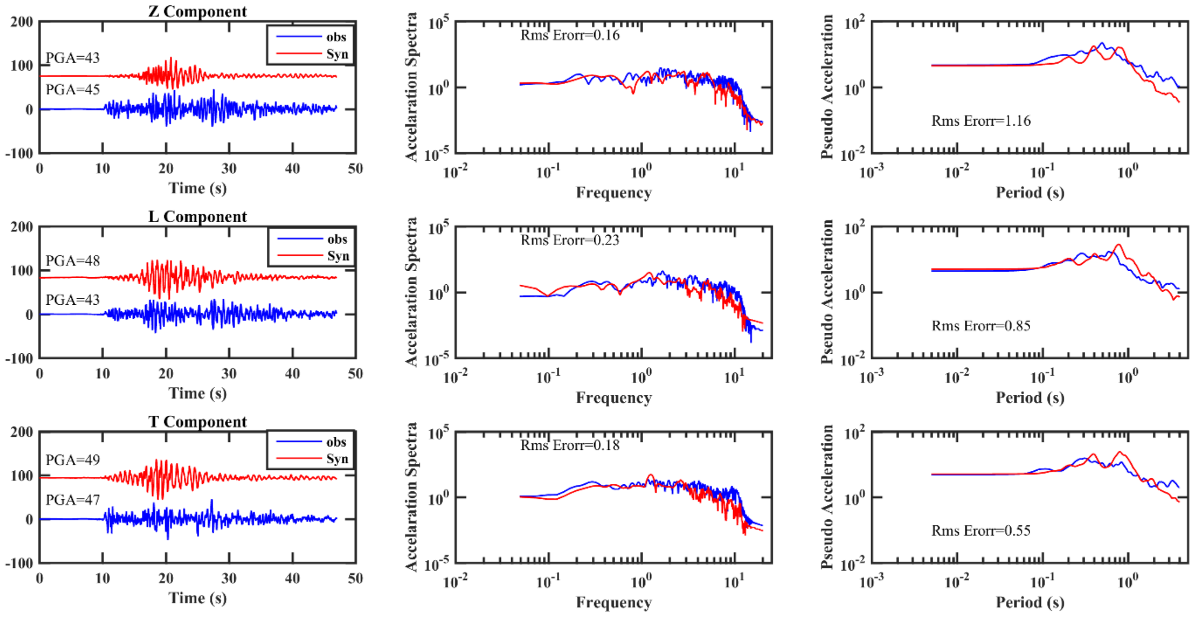

Fig 8. Observed and simulated time series for Nosood station; Acceleration spectrum and response spectrum also shown for observed (blue lines) and simulated (red lines) time series.

The results of the parameters obtained are in good agreement with the Iranian Seismological Center (IRSC) reported results as well. As it can be seen in Figures 6 to12 the PGA of the simulated records is in good agreement with the observed values; also the amplitude spectrum and response of the observed and synthetic records also have good agreement over a wide frequency range. Earthquake durability is another effective parameter in engineering studies. The simulation results show that the durability parameter in the simulated records are in good agreement with the observed records as well.

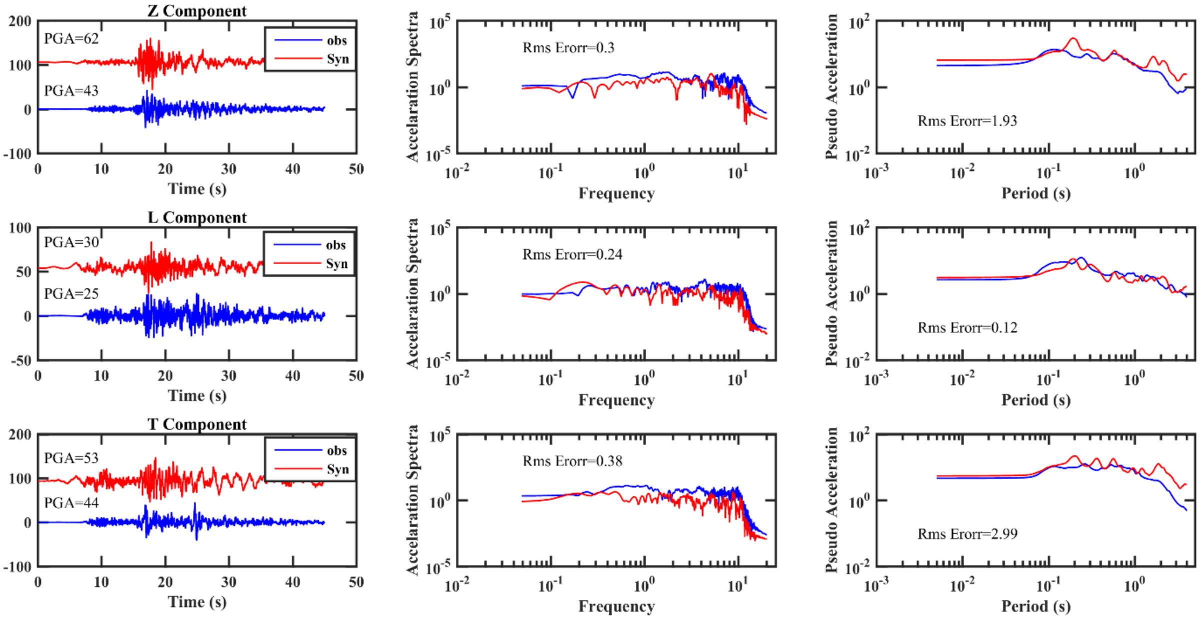

Fig 9. Observed and simulated time series for Palangan station; Acceleration spectrum and response spectrum also shown for observed (blue lines) and simulated (red lines) time series.

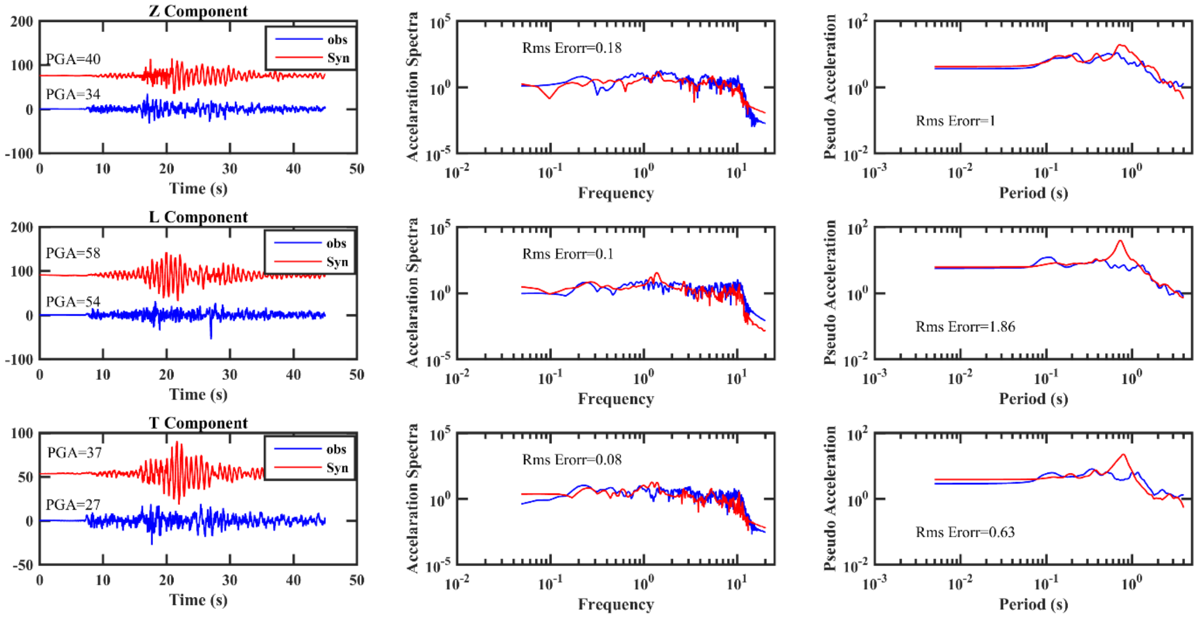

Fig 10. Observed and simulated time series for Sarv-Abad station; Acceleration spectrum and response spectrum also shown for observed (blue lines) and simulated (red lines) time series.

However, the EGF method shows that the results of this method are strongly dependent on the selection of records used as the EGF, which is a major problem in utilizing the EGF method. If the selected record is not an appropriate record, it can produce the wrong information from the propagation path and site effects and affects the final results. Figure 13 shows the observed and calculated PGA values versus the epicentral distance for the vertical components. As shown in Figure 13, the maximum recorded PGA was observed at the Sarpol-e zahab station, which has the shortest distance from the earthquake focal point. Generally, when the distance increases, the PGA values decrease.

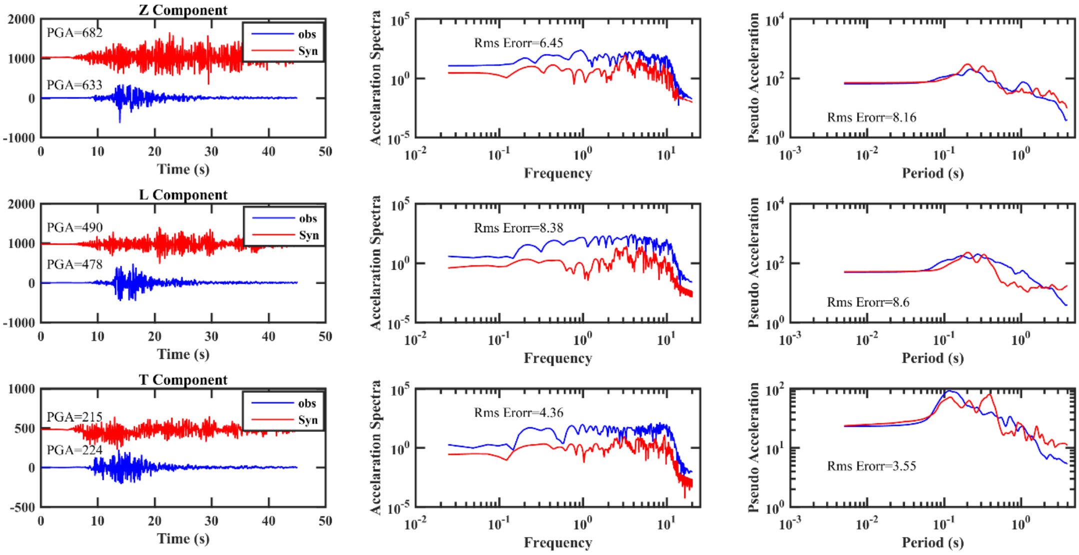

Fig 11. Observed and simulated time series for Sarpolezahab station; Acceleration spectrum and response spectrum also shown for observed (blue lines) and simulated (red lines) time series.

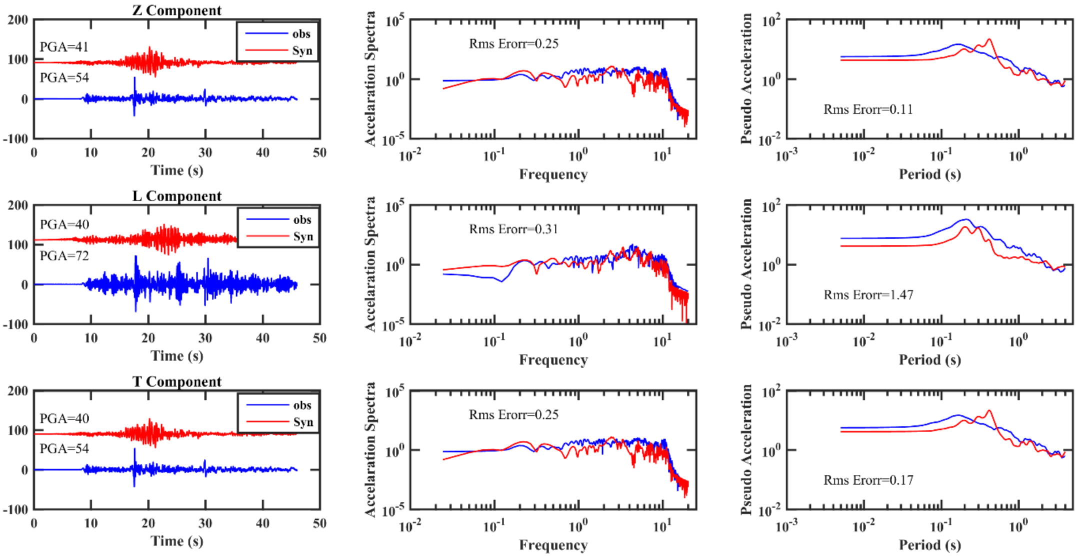

Fig 12. Observed and simulated time series for Shoeisheh station; Acceleration spectrum and response spectrum also shown for observed (blue lines) and simulated (red lines) time series.

The PGA values at Palangan Station is greater than that of Nosood and the PGA values at Marivan Station is greater than that of Sarv-Abad station. This situation can be seen in both observational and computational graphs. Based on the Code (2005) and reported results by Zare et al. (1999), all station which are used in this study, is located on soil class II. Therefore, the greater PGA value at greater distance may be due to the difference in path (velocity and attenuation) effect, or the nonlinearity in site response.

In this step, the acceleration design spectrum of each simulated acceleration was determined. For this sake, initial corrections (baseline correction, selection of the correction frequency, and band pass filter) were applied on each record and then, the acceleration linear response spectrum were calculated for horizontal components (L component) of the records with 5% damping (Code 2005). After that, we normalized the obtained spectra to the maximum acceleration of the Earth's motion. Finally, we compared the obtained results with acceleration design spectrum Code (2005) (Fig 14).

According to the Code (2005) and Zare et al. (1999) the selected stations in this study are located on soil which classified as soil class II. Shear wave velocity in this type of soil is between 350 to 750 m/s (Code 2005). For this sake, we compared estimated acceleration design spectrum in different stations with the same spectrum in soil class II of Code (2005) (Fig 14). Figure 14 shows that the simulated acceleration design spectra at Sarpol-e zahab station is clearly above the 2800-code range in short period. This higher value of acceleration design spectra has been reported in observed spectral responses of the Sarpol-e zahab station (Shahvar et al. 2018), which suggests the reevaluation the code of practice for that area. For other stations, the results are in good agreement with Code (2005) for all station (Fig 14). The results show that when appropriate small events are available in an area, the EGF method is a good method for simulating the strong motion caused by the main shock, as well as studying of the seismological parameters of that area. Therefore, in an area where the records of the strong ground motion are not available or are scattered, or the recorded strong ground motion data have good quality, with the simulation of the strong ground motion in that specific site, the vital information for important studies such as the study of the seismic potential of the area, study of the mechanism of earthquakes, and earthquake hazard analysis can be provided in order to reduce the life casualties and financial losses during the large major earthquakes.

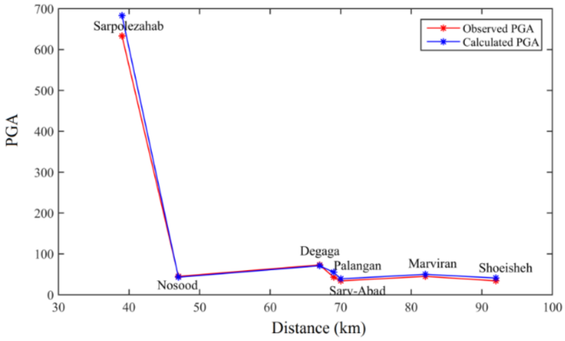

Fig 13. Observed and calculated PGA (sm/s^2) values versus the epicentral distance. Blue stars are PGA (sm/s^2) obtained from synthetic waveforms and red stars are PGA obtained from observed waveforms.

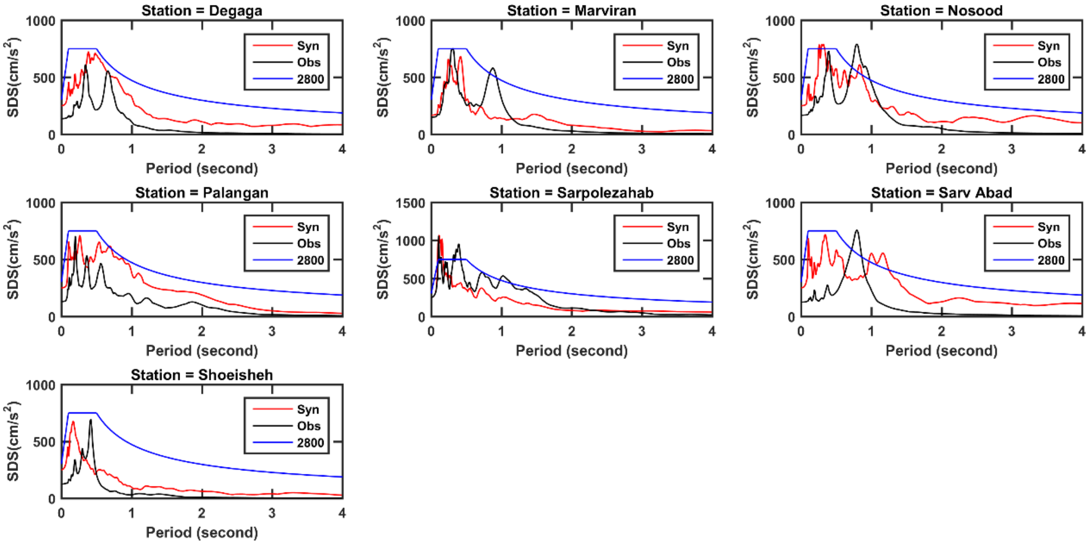

Fig 14. Comparison between acceleration design spectrum of simulated records (red line); observed record (black line) and acceleration design spectrum of Code (2005) (blue line).

References

Ahmadi A, Bazargan-Hejazi S (2018) 2017 Kermanshah earthquake; lessons learned, *Journal of injury and violence research* 10:p1.

Ambraseys N, Melville C (1982) A History of Persian Earthquakes ,Cambridge University Press. London.

Bazoobandi MH, Arian MA, Emami MH, Tajbakhsh G, Yazdi A (2016) Petrology and Geochemistry of dikes in the North of Saveh in Iran. *Open journal of marine science* 6(2) 210-222.

Boore DM (1983) Stochastic simulation of high-frequency ground motions based on seismological models of the radiated spectra, *Bulletin of the Seismological Society of America* 73:1865-1894.

Boore DM (2003) Simulation of ground motion using the stochastic method, *Pure and applied geophysics* 160:635-676.

Bouchon M, Hatzfeld D, Jackson JA, Haghshenas E (2006) Some insight on why Bam (Iran) was destroyed by an earthquake of relatively moderate size, *Geophysical Research Letters* 3:p9.

Code IS (2005) Iranian code of practice for seismic resistant design of buildings, *Standard*.

Ding K, He P, Wen Y, Chen Y, Wang D, Li S, Wang Q (2018) The 2017 M w 7.3 Ezgeleh, Iran earthquake determined from InSAR measurements and teleseismic waveforms, *Geophysical Journal International* 215:1728-1738.

Dewey JF, PITMAN WC III, Ryan WB, Bonnin J (1973) Plate tectonics and the evolution of the Alpine system, *Bull. geol. Soc. Am* 84(10), 3137–3180.

Falcon NL (1974) Southern Iran: Zagros Mountains, *Geological Society, London, Special Publications* 4:199-211.

Feng W, Samsonov S, Almeida R, Yassaghi A, Li J, Qiu Q, Li P, Zheng W (2018) Geodetic Constraints of the 2017 Mw7. 3 Sarpol Zahab, Iran Earthquake, and Its Implications on the Structure and Mechanics of the Northwest Zagros Thrust-Fold Belt, *Geophysical Research Letters* 45:6853-6861.

Gombert B, Duputel Z, Shabani E, Rivera L, Jolivet R, Hollingsworth J (2019) Impulsive Source of the 2017 MW= 7.3 Ezgeleh ,Iran, Earthquake, *Geophysical Research Letters* 46:5207-5216.

Hartzell SH (1978) Earthquake aftershocks as Green's functions, *Geophysical Research Letters* 5:1-4.

Irikura K Prediction of strong acceleration motion using empirical Green’s function. In: Proc٧ .th Japan Earthq. Eng. Symp, 1986. pp 151-156.

Irikura K, Miyake H (2011) Recipe for predicting strong ground motion from crustal earthquake scenarios, *Pure and Applied Geophysics* 168:85-104.

Jackson J, Haines J, Holt W (1995) The accommodation of ArabiaEurasia plate convergence in Iran, *Journal of Geophysical Research:Res: Solid Earth* 100(B8): 15205–15219.

Kanamori H, Anderson DL (1975) Theoretical basis of some empirical relations in seismology, *Bulletin of the seismological society of America* 65:1073-1095.

Kaviani A (2004) La châin de collision continentale du Zagros (Iran): structure lithosphérique par analyse de données sismologique .

Madariaga R (1976) Dynamics of an expanding circular fault, *Bulletin of the Seismological Society of America* 66:639-666.

Miyake H, Iwata T, Irikura K (2003) Source characterization for broadband ground-motion simulation: Kinematic heterogeneous source model and strong motion generation area, *Bulletin of the Seismological Society of America* 93:2531-2545.

Miyamjima M, Fallahi A, Ikemoto T, Samaei M, Karimzadeh S, Setiawan H, Talebi F, Karashi J (2018) Site investigation of the Sarpole-Zahab earthquake, Mw 7.3 in SW Iran of November 12 , *JSCE J Disaster FactSheets*.

Niño M, Ayala G, Ordaz M (2018) Ground-Motion Simulation by the Empirical Green’s Function Method with a Source Defined by Two Corner Frequencies and a Two-Stage Summation SchemeGround-Motion Simulation by the EGF Method, *Bulletin of the Seismological Society of America* 2018 Apr 1;108(2):901-12.

Nicknam A, Abbasnia R, Eslamian Y, Bozorgnasab M (2009) Extrapolating strong ground motion of the Silakhor earthquake (ML 6.1), Iran, using the empirical Green's function (EGF) approach based on a genetic algorithm, *Canadian Journal of Earth Sciences* 46:801-810.

Poorbehzadi K, Yazdi A, Sharifi Teshnizi E, Dabiri R (2019) Investigating of Geotechnical Parameters of Alluvial Foundation in Zaram-Rud Dam Site, North Iran. *International Journal of Mining Engineering and Technology* 1(1): 33-34.

Riahi A, Sadeghi H, Hosseini SK (2015) Simulation of 2003 Bam (Iran) earthquake using empirical Green's function method via very small and near-fault events, *Geophysical Journal International* 201:1264-1286.

Shahvar MP, Eshaghi A, Farzanegan E, Alavijeh HM (2018) StrongMotion Records in Sarpol-e-Zahab Earthquake, *Journal of Seismology & Earthquake Engineering* 20.

Somerville P, Irikura K, Graves R, Sawada S, Wald D, Abrahamson N, Iwasaki Y, Kagawa T, Smith N, Kowada A (1999) Characterizing crustal earthquake slip models for the prediction of strong ground motion, *Seismological Research Letters* 70:59-80.

Tatar M (2001) Etude sismotectonique de deux zones de collision continentale: le Zagros central et l'Alborz (Iran) .Grenoble 1.

Theodulidis N, Bard PY (1995) Horizontal to vertical spectral ratio and geological conditions: an analysis of strong motion data from Greece and Taiwan (SMART-1), *Soil dynamics and earthquake engineering* 14(3): 177-197.

Vajedian S, Motagh M, Mousavi Z, Motaghi K, Fielding E, Akbari B, Wetzel HU, Darabi A (2017) Coseismic deformation field of the Mw 7.3 12 November 2017 Sarpol-e Zahab (Iran) earthquake: A decoupling horizon in the northern Zagros Mountains inferred from InSAR observations, *Remote Sensing* 2018 Oct;10(10):1589.

Yazdi A, Ashja-Ardalan A, Emami MH, Dabiri R, Foudazi M (2017) Chemistry of Minerals and Geothermobarometry of Volcanic Rocks in the Region Located in Southeast of Bam, Kerman Province. *Open Journal of Geology* 7(11): 1644-1653.

Yazdi A, Shahhosini E, Dabiri R, Abedzadeh H (2019) Magmatic differentiation evidences and source characteristics using mineral chemistry in the Torud intrusion (Northern Iran), *Revista Geoaraguaia* 9(2): 1-21.

Zare M, Bard P-Y, Ghafory-Ashtiany M (1999) Site characterizations for the Iranian strong motion network, *Soil Dynamics and Earthquake Engineering* 18:101-123.